The ^{7}Li($\vec{d}$, n_0)^{8}Be and ^{7}Li($\vec{d}$, n_1)^{8}Be reactions below 160 keV

A. Sabourov, M. W. Ahmed, M. A. Blackston, A. S. Crowell, C. R. Howell, K. Joshi, S. O. Nelson, B. A. Perdue, K. Sabourov, A. Tonchev, and H. R. Weller
Department of Physics, Duke University, Durham, North Carolina 27708, USA and Triangle Universities Nuclear Laboratory, Durham, North Carolina 27708, USA

R. M. Prior and M. C. Spraker
North Georgia College and State University, Dahlonega, Georgia 30597, USA and Triangle Universities Nuclear Laboratory, Durham, North Carolina 27708, USA

B. Braizinha
Triangle Universities Nuclear Laboratory, Durham, North Carolina 27708, USA

N. Kalantar-Nayestanaki
KVI, University of Groningen, Groningen, The Netherlands
(Received 25 August 2006; published 18 December 2006)

The polarization observables have been determined for the ^{7}Li($\vec{d}$, n_0)^{8}Be and ^{7}Li($\vec{d}$, n_1)^{8}Be reactions at beam energies between 80 and 160 keV. A Transition Matrix Element (TME) analysis revealed unique, dominant p-wave solutions for both neutron channels. The polarization observables were compared with distorted wave Born approximation (DWBA) and coupled reaction channels (CRC) calculations. The general features of the data can be reproduced by the CRC calculations when a large target spin-orbit interaction is included. However, serious discrepancies are observed when the TMEs of the theory and experiment are compared.

DOI: 10.1103/PhysRevC.74.064611 PACS number(s): 27.20.+n, 24.70.+s, 25.45.Hi

I. INTRODUCTION

The primordial abundance of ^{7}Li is one of the more important diagnostics of the degree of baryon inhomogeneity in early universe models [1]. The ^{7}Li yield is determined from a balance between production and destruction reactions. An accurate knowledge of both types of reactions is necessary for cosmological model calculations to be reliable.

In general, the ^{7}Li(d, n)^{8}Be reaction is not well understood at very low energies. Very little experimental data are available below several hundred keV [2], especially data investigating the vector and tensor analyzing powers which result from polarized deuteron beams on the ^{7}Li target. These analyzing powers provide detailed information about the reaction dynamics which enable theorists to test interaction models.

The polarization observables can be compared directly to the observables predicted by theoretical calculations. However, this comparison only reveals major differences between theory and experiment; greater insight can be obtained by investigating the origins of these differences. One powerful way to do this is to expand the observables in terms of the complex transition matrix elements (TMEs). The amplitudes and phases of the TMEs can be fitted to the measured data to obtain the values that best represent the data. This provides a deeper insight into the reaction mechanisms themselves: critical information about why the theory and experiment may differ can be gleaned by comparing these TMEs with those calculated from theory.

The lowest energy measurement of the polarization observables previously reported for the ^{7}Li($\vec{d}$, n_0)^{8}Be reaction was performed by von Möllendorf *et al*. at 640 keV [3]. They measured the angular distribution of the analyzing powers between 0° and 160° for the n_0 group and performed a TME analysis, determining that the reaction proceeds primarily by s-waves and p-waves in the entrance channel at these energies. Unfortunately, the measurement is at an energy too high to compare with the present work.

The work presented here consists of polarization observable measurements. The experimental polarization observables were compared with both distorted wave Born approximation (DWBA) and coupled reaction channels (CRC) calculations. Because the CRC calculation gave a reasonable description of the polarization observables, the model's prediction for the behavior of the contributing transition matrix elements (TMEs) was compared with those that were obtained from a detailed TME analysis of the experimental data in an energy region between $E_{\mathrm{c.m.}} = 62$ keV and 124 keV. Absolute cross section and astrophysical S-factor measurements for these reactions were presented in Ref. [4].

II. EXPERIMENTAL METHOD

The Triangle Universities Nuclear Laboratory (TUNL) atomic beam polarized ion source (ABPIS) produced vector and tensor polarized deuteron beams for polarization observable measurements. In addition to measurements being performed at $E_d = 80$ keV, the 80-keV deuterons from the ABPIS were accelerated to 130 keV and 160 keV by biasing the target chamber. Beam currents averaged about 20 μA on target.

The target was made *in situ* in the vacuum chamber. Enriched 99% ^{7}Li was evaporated directly onto the

3-mm-thick aluminum target chamber face and was replenished every 8 h. The emitted neutrons were detected using six 12.7-cm diameter and three 11.4-cm diameter organic liquid scintillators containing BC-501 fluid. Detectors were placed approximately 43 cm from the target face at nine angles between 0° and 150°. Data acquisition was configured to utilize pulse-shape discrimination (PSD) to enable separation of the neutrons from the gamma-ray background. The target and detectors, as well as the yield-extraction procedure, are described in greater detail in Ref. [4].

The beam polarization and analyzing powers are typically considered with respect to the Madison Convention coordinate system [5]. It is convenient to express the beam polarization with respect to an internal coordinate system in which the third axis is the spin-symmetry axis of the beam $\hat{\zeta}$. In this system, most of the polarization moments related to the spin-state occupation numbers vanish to leave only p_ζ and $p_{\zeta\zeta}$, and the spin-symmetry axis direction is given by angles β and ϕ. The cross section can then be written in terms of the detector angle θ as

$$\begin{aligned}\sigma(\theta) = \sigma_0(\theta)\Bigg(1 &+ \sqrt{3}p_\zeta i T_{11}(\theta)\sin\beta\cos\phi \\ &+ \frac{1}{2\sqrt{2}}p_{\zeta\zeta}T_{20}(\theta)(3\cos^2\beta - 1) \\ &+ \sqrt{3}p_{\zeta\zeta}T_{21}(\theta)\sin\beta\cos\beta\sin\phi \\ &- \frac{\sqrt{3}}{2}p_{\zeta\zeta}T_{22}(\theta)\sin^2\beta\cos 2\phi\Bigg). \end{aligned} \quad (1)$$

The ABPIS produces polarized beams with specific values of p_ζ and $p_{\zeta\zeta}$, while allowing the spin-symmetry axis to be rotated by means of a Wien filter. Through appropriate selection of specific beam polarizations and polarization axis alignments, the above equation can be used to extract an analyzing power of interest.

The vector analyzing power $iT_{11}(\theta)$ can be found by using a purely vector-polarized beam that has $\beta = 90°$ and $\phi = 0°$ and switches p_ζ between the two polarization states p_z^+ and $-p_z^-$, where both p_z^+ and p_z^- are positive quantities and have an ideal value of +1. Placing these values in Eq. (1) gives

$$iT_{11}(\theta) = \frac{1}{\sqrt{3}}\frac{Y_+(\theta) - Y_-(\theta)}{Y_+(\theta)p_z^- + Y_-(\theta)p_z^+}, \quad (2)$$

where Y_- and Y_+ are the yields for a beam with polarization $p_\zeta = -p_z^-$ and p_z^+, respectively. Using a tensor-polarized beam which has $\beta = 0°$ and switches between polarization states $p_{\zeta\zeta} = p_{zz}^+$ and $-p_{zz}^-$, where p_{zz}^+ and p_{zz}^- are both positive quantities, gives

$$T_{20}(\theta) = \sqrt{2}\left(\frac{Y_+(\theta) - Y_-(\theta)}{Y_+(\theta)p_{zz}^- + Y_-(\theta)p_{zz}^+}\right). \quad (3)$$

The observable $T_{22}(\theta)$ can be measured by choosing a pure tensor polarized beam, with $p_\zeta = 0$, $p_{\zeta\zeta} = p_{zz}^+$ and $-p_{zz}^-$, and $\beta = 54.7°$ and $\phi = 0°$. This choice leads to

$$T_{22}(\theta) = -\sqrt{3}\frac{Y_+(\theta) - Y_-(\theta)}{Y_+(\theta)p_{zz}^- + Y_-(\theta)p_{zz}^+}. \quad (4)$$

The observable $T_{21}(\theta)$ is the hardest of the five observables to measure. An asymmetry between left and right detectors for three spin states was required: $p_{\zeta\zeta} = p_{zz}^+$, $p_{\zeta\zeta} = -p_{zz}^-$, and an unpolarized ($p_{\zeta\zeta} = 0$) state. The angle β was set to 45°, and detectors at beam right had $\phi = 90°$ and those on beam left had $\phi = -90°$. Equation (1) then becomes

$$\begin{aligned}L(\theta) = \frac{Y(\theta, -90°)}{Y_0(\theta)} &= 1 + \frac{1}{4\sqrt{2}}p_{\zeta\zeta}T_{20}(\theta) \\ &- \frac{\sqrt{3}}{2}p_{\zeta\zeta}T_{21}(\theta) + \frac{\sqrt{3}}{4}p_{\zeta\zeta}T_{22}(\theta) \end{aligned} \quad (5)$$

and

$$\begin{aligned}R(\theta) = \frac{Y(\theta, 90°)}{Y_0(\theta)} &= 1 + \frac{1}{4\sqrt{2}}p_{\zeta\zeta}T_{20}(\theta) \\ &+ \frac{\sqrt{3}}{2}p_{\zeta\zeta}T_{21}(\theta) + \frac{\sqrt{3}}{4}p_{\zeta\zeta}T_{22}(\theta), \end{aligned} \quad (6)$$

where $L(\theta)$ and $R(\theta)$ correspond to the yields for the beam left and beam right detectors respectively, and $Y(\theta, \pm 90°)$ and $Y_0(\theta)$ are the polarized and unpolarized yields, respectively, for the detector at angle θ. Solving these two equations for $T_{21}(\theta)$ gives

$$T_{21}(\theta) = \frac{1}{\sqrt{3}}\frac{R(\theta) - L(\theta)}{p_{\zeta\zeta}}. \quad (7)$$

Detector pairs were periodically swapped from beam left to beam right to reduce systematic errors. In addition, the $T_{21}(\theta)$ for the p_{zz}^+ and p_{zz}^- states were averaged.

The beam polarization must be reliably known in order to obtain accurate values of the analyzing powers. The spin filter polarimeter (SFP) allows for tuning the ABPIS to maximum polarization. The SFP values are known to differ by less than 5% with respect to the values measured using other polarimeters located at the high-energy end of the tandem [6]. These values were used in producing the analyzing powers reported in this paper.

III. TRANSITION MATRIX ELEMENT ANALYSIS

The cross section and analyzing powers can be expressed in terms of Legendre polynomials such that [7]

$$\begin{aligned}\sigma_0(\theta) &= A_0\left(1 + \sum_{k=1} Q_k a_k P_k(\cos\theta)\right), \\ iT_{11}(\theta)\sigma_0(\theta) &= \frac{A_0}{\sqrt{3}}\sum_k Q_k b_k P_k^1(\cos\theta), \\ T_{20}(\theta)\sigma_0(\theta) &= A_0\sum_k Q_k c_k P_k(\cos\theta), \\ T_{21}(\theta)\sigma_0(\theta) &= \frac{A_0}{2}\sum_k Q_k d_k P_k^1(\cos\theta), \quad \text{and} \\ T_{22}(\theta)\sigma_0(\theta) &= \frac{A_0}{2}\sum_k Q_k e_k P_k^2(\cos\theta), \end{aligned} \quad (8)$$

where $\sigma_0(\theta)$ is the unpolarized cross section and Q_k corrects for finite geometry. The angle integrated cross section σ_T is given by $\sigma_T = 4\pi A_0$.

The coefficients of the Legendre polynomial expansions can be related to the complex transition matrix elements (TMEs). The significance of various Legendre polynomials in the expansion gives a hint as to which transitions will be involved in the reaction. The data were fitted to a Legendre polynomial expansion using a least-squares fit method as described in detail in Ref. [8]. (The results of these fits are listed in Tables VII and VIII of the Appendix.)

General expressions for the reaction cross section in terms of Legendre polynomials and the contributing TMEs show that, on the basis of angular momentum coupling theory, the highest order polynomial which appears in the expansion is given by $k_{\max} \leqslant 2\ell$ or $k_{\max} \leqslant 2\ell'$, whichever is smaller [9], where ℓ is the orbital angular momentum for the incoming $(^7\mathrm{Li} + d)$ channel and ℓ' is that for the outgoing $(^8\mathrm{Be} + n)$ channel. The best fit of the ^{7}Li$(\vec{d}, n_0)^8$Be data to a Legendre polynomial expansion went to order $k = 4$ for all observables except $\sigma_{\mathrm{c.m.}}$, for which an expansion to $k = 3$ was sufficient. The need to expand to $k = 3$ arises from an interference between $\ell = 1$ and $\ell = 2$ terms and indicates that some d-waves ($\ell = 2$) need to be included in the TME expansion for this channel; these d-waves can also generate the $k = 4$ terms in the analyzing powers. An expansion to order $k = 2$, however, produced the best fit to the ^{7}Li$(\vec{d}, n_1)^8$Be data. Increasing the expansion to order $k = 3$ did not reduce the χ^2/ν value or add any additional significant terms. This indicates that only s- and p-waves ($\ell \leqslant 1$) need be considered in the TME expansion for this channel.

The expansion of the Legendre polynomial coefficients in terms of reaction TMEs is done according to the formalism of Ref. [7] where each TME is written in the form of $\mathrm{R} = |\mathrm{R}|\, e^{i\phi}$ where $|\mathrm{R}|$ is the TME amplitude and ϕ is its phase. In the case of the ^{7}Li$(\vec{d}, n_0)^8$Be reaction, the entrance channel can be limited to s-, p-, and d-waves, i.e., $\ell = 0$, 1, and 2. The initial TMEs were further constrained by limiting $\ell' \leqslant 3$ since higher values of ℓ' are expected to be smaller on the basis of angular momentum barrier effects. This results in twenty matrix elements and nineteen relative phases. In order to reduce this to manageable numbers, elements with the same s, ℓ, and ℓ' values but different J and s' values were set to be equal to one another. This is done assuming that the coupling of ℓ and s, most of which arises from the spin-orbit effects, is small compared to the ℓ and s dependence itself. Finally, the phases are assumed to be determined from the ℓ-values and were therefore limited to a relative p- to s-wave phase ϕ_{p-s} and a relative d- to p-wave phase ϕ_{d-p}, as well as a phase δ^s between s-wave elements with $\ell' = 1$ and $\ell' = 3$, a phase δ^p between p-wave elements with $\ell' = 0$ and $\ell' = 2$, and a phase δ^d between d-wave elements with $\ell' = 1$ and $\ell' = 3$. Spin-dependent effects, expected to be less important than the ℓ-dependent effects, are neglected by doing this. This results in fourteen TMEs and five phases for a total of nineteen independent parameters to fit to the data. Ultimately, the ability to fit the data with this reduced set of amplitudes and phases will be used to justify these simplifications.

From the Legendre polynomial fits described previously, only s- and p-waves, i.e., $\ell = 0$ and 1, need to be considered in the entrance channel for ^{7}Li$(\vec{d}, n_1)^8$Be. The initial set of TMEs were further constrained by limiting $\ell' \leqslant 2$ and $J \leqslant 5/2$, again since higher values of ℓ' and J are expected to be smaller on the basis of angular momentum barrier effects. This results in 24 matrix elements and 23 relative phases. For the same reasons given for the n_0 state TME reduction, the n_1 state TMEs were constrained by equating all elements with the same s, ℓ, and ℓ' values. In addition, only two phases were considered: a relative p- to s-wave phase ϕ_{p-s} and a phase δ^p between p-wave elements with $\ell' = 0$ and $\ell' = 2$. This results in a total of nine TMEs and two phases for a total of 11 independent parameters to fit to the data.

The formalism of Welton [10] and Devons and Goldfarb [11] was used to relate the TMEs to the Legendre polynomial coefficients. The expressions which relate the Legendre polynomial coefficients of each observable to the various TMEs specified by the user were obtained from the FORTRAN code FATSO [12] written by Seiler. Equations for the Legendre polynomial coefficients in terms of the constrained TMEs and phases are then inserted into the Legendre polynomial expansions. The amplitudes and phases are then searched on to find the best fit to the observables simultaneously. This is done by performing a least-square minimization procedure to all data points. Grid searches for the best fit of the TME amplitudes and phases to the full data set at $E_d = 160$ keV were performed. Each amplitude was initially set to 100% while the other amplitudes were set to zero, and for that set of amplitudes, each phase was individually varied in 60° steps while the others remained the same. These starting values for the amplitudes and phases were then searched on to obtain the best fit. The resulting solutions with the lowest total χ^2 were searched on again, varying the amplitudes and phases in each case. The three best solutions from the $E_d = 160$ keV searches were then searched on at $E_d = 130$ keV and 80 keV. For both the ^{7}Li$(\vec{d}, n_0)^8$Be and ^{7}Li$(\vec{d}, n_1)^8$Be data sets, these three solutions, which were all similar, collapsed to a single solution at lower energies. In comparison, the next "best" solution for the ^{7}Li$(\vec{d}, n_0)^8$Be reaction at $E_d = 160$ keV had a $\chi^2/\nu = 24.6$ as compared to a value of 1.0 for the best solution. For the ^{7}Li$(\vec{d}, n_1)^8$Be reaction at this energy, the next "best" fit had a $\chi^2/\nu = 5.2$ compared to 3.2 for the best solution.

The results of the TME fits to the ^{7}Li$(\vec{d}, n_0)^8$Be data are given in Table I, where the TMEs are labeled using the notation $^{2s+1}\ell_{2J+1}$, and the TME fits to the data are shown in Figs. 1–3. In the table, more than one entry in Column 1 indicates that these TMEs were set equal to one another in our analysis. The solution is comprised of over 70% p-waves, with the $^2p_2$ matrix element dominating. S-wave and d-wave components make up about 10% each of the total solution for $E_d = 160$ keV, but at the lower beam energies, the d-wave component falls to less than 5% and the p-wave component rises to over 80%.

Table II shows the results of the TME fits to the ^{7}Li$(\vec{d}, n_1)^8$Be data as a function of energy. Because elements with the same ℓ, s, and J values can have different ℓ' and s'

TABLE I. Results of the TME fits to the ^{7}Li$(\vec{d}, n_0)^8$Be data.

E_d = TME	160 keV	130 keV	80 keV
		Strength (%)	
$^2s_2$	11 ± 2	8 ± 1	11 ± 1
$^2p_2$	49 ± 8	61 ± 9	62 ± 3
$^4p_2$	13 ± 3	11 ± 3	4 ± 1
$^2p_4$	0.04 ± 0.1	1 ± 0.5	0.01 ± 0.02
$^4p_4, ^4p_6$	12 ± 2	12 ± 2	14 ± 1
$^6p_4, ^6p_6$	1 ± 0.4	2 ± 0.8	4 ± 1
$^2d_4$	0.01 ± 0.01	0.01 ± 0.05	1 ± 0.2
$^4d_6$	1 ± 0.6	0.01 ± 0.06	0.01 ± 0.05
$^6d_6$	0.01 ± 0.1	1 ± 0.9	0.5 ± 0.5
$^2d_6$	13 ± 4	4 ± 2	3 ± 0.3
		Phase (°)	
ϕ_{p-s}	-75 ± 4	-78 ± 4	-46 ± 1
ϕ_{d-p}	174 ± 4	172 ± 4	118 ± 2
δ^s	0 ± 525	0 ± 538	0 ± 537
δ^p	-44 ± 10	-46 ± 14	-47 ± 6
δ^d	-20 ± 35	150 ± 38	0 ± 50
χ^2_ν	1.0	0.9	1.6

values, some elements may have the same $^{2s+1}\ell_{2J+1}$ notation. In these cases, the differing values of s' or ℓ' are noted in parentheses. For example, an element listed as $^4s_4(s' = 3/2, 5/2)$ is actually two elements that have been set equal to one another: the $^4s_4$ element with $s' = 3/2$ and the $^4s_4$ element with $s' = 5/2$. Each observable is graphed with the TME fit to the data in Figs. 4–6. As can be seen from these figures and Table II, p-waves dominate the solution, especially at 80 keV, where they comprise almost 100% of the total contribution. The $^6p_4$ and $^6p_6$ matrix elements together, which we set equal to one another in our analysis, dominate. Each amplitude's percentage contribution to the total strength is weighed by $2J + 1$. This weighting means that, for $E_d = 160$ keV, the $^6p_4$ element contributed 17% and the $^6p_6$ element contributed 25% of the total strength for a total of 42%; for $E_d = 130$ keV, they contributed 21% and 31%, respectively, for a total of 52%; and for $E_d = 80$ keV, they contributed 22% and 32%, respectively, for a total of 54%. However, the increase in the χ^2-values for the higher energies may indicate that our simplifying assumptions are breaking down at these energies.

TABLE II. Results of the TME fits to the ^{7}Li$(\vec{d}, n_1)^8$Be data.

E_d = TME	160 keV	130 keV	80 keV
		Strength (%)	
$^2s_2$	21 ± 4	19 ± 11	0.2 ± 2
$^4s_4$ ($s' = 3/2, 5/2$)	25 ± 4	0.01 ± 0.3	0.02 ± 17
$^6s_6$ ($s' = 3/2, 5/2$)	1 ± 0.3	14 ± 7	0.2 ± 8
$^4p_4, ^4p_6$	6 ± 2	7 ± 4	19 ± 6
$^6p_4, ^6p_6$	42 ± 6	52 ± 10	54 ± 15
$^6p_4$ ($s' = 3/2, 5/2$), $^6p_6$ ($s' = 3/2, 5/2$)	5 ± 1	8 ± 4	27 ± 10
		Phase (°)	
ϕ_{p-s}	153 ± 3	146 ± 5	179 ± 63
δ^p	-168 ± 8	-153 ± 17	-171 ± 14
χ^2_ν	3.2	1.6	0.6

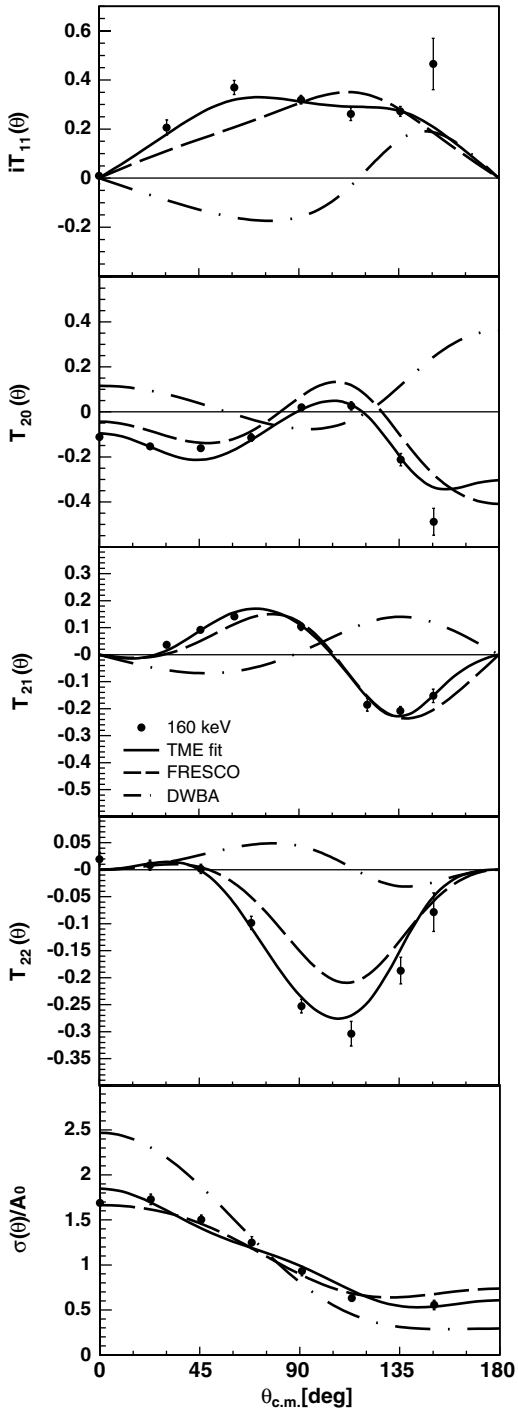

FIG. 1. Experimental data for the ^{7}Li$(\vec{d}, n_0)^8$Be reaction at $E_d = 160$ keV with the results of a TME fit (solid line), the FRESCO calculations (dashed line), and the DWBA calculation (dash-dotted line). The error bars represent the statistical and systematic uncertainties.

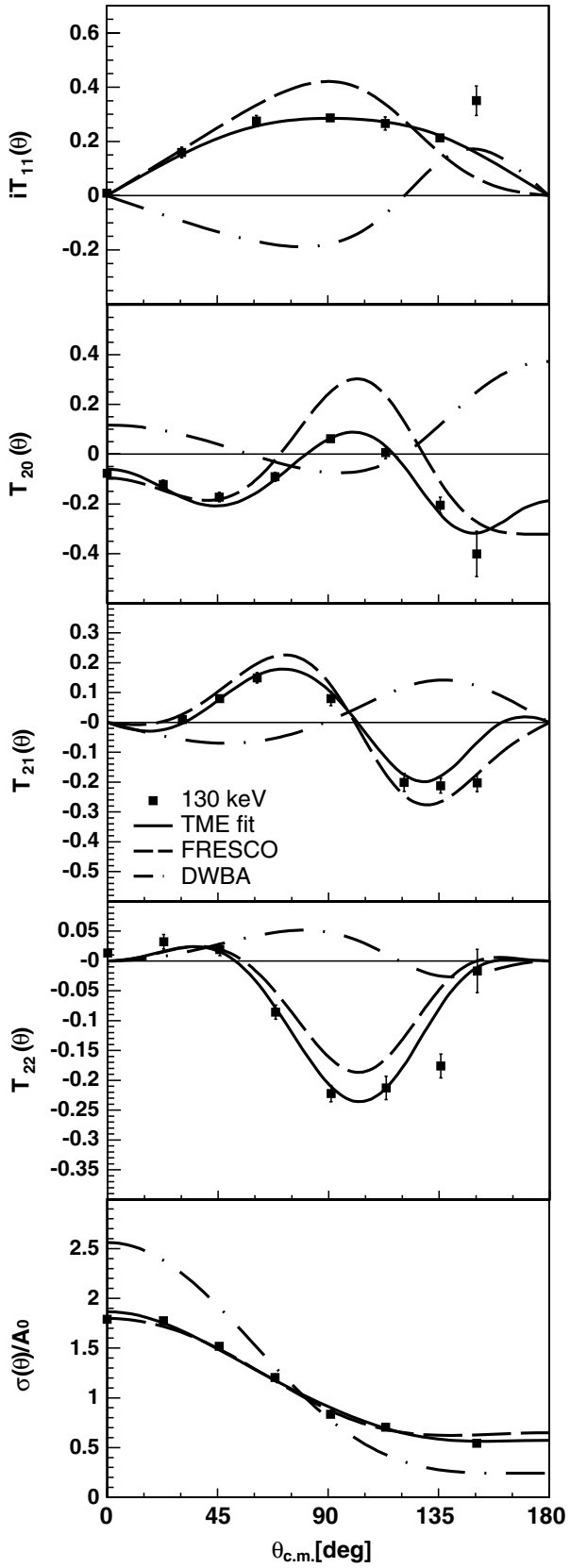

FIG. 2. Experimental data for the ^{7}Li($\vec{d}, n_0$)^{8}Be reaction $E_d =$ 130 keV with the results of a TME fit (solid line), the FRESCO calculations (dashed line), and the DWBA calculation (dash-dotted line). The error bars represent the statistical and systematic uncertainties.

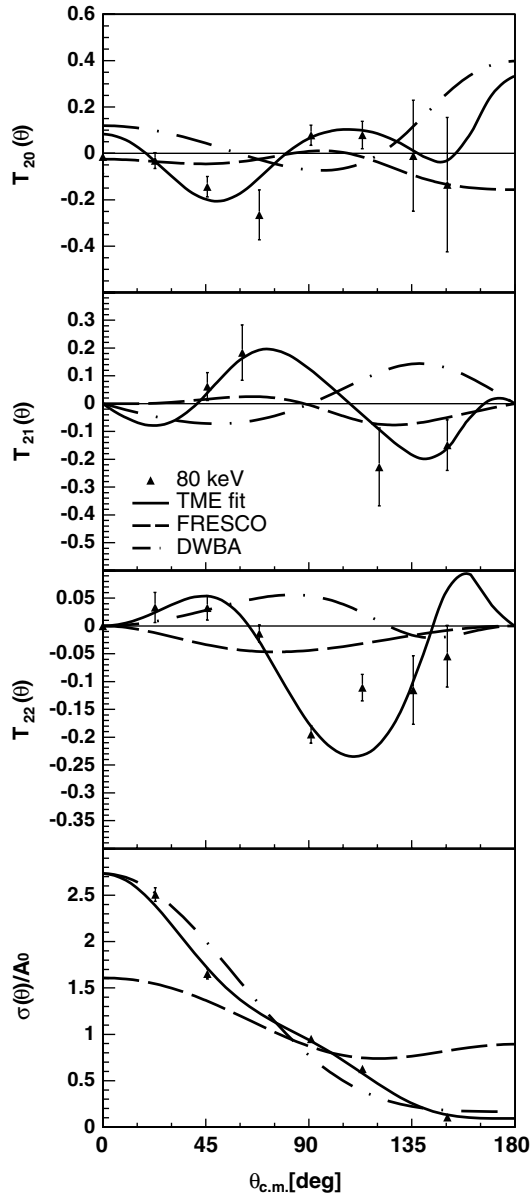

FIG. 3. Experimental data for the ^{7}Li($\vec{d}, n_0$)^{8}Be reaction at $E_d = 80$ keV with the results of a TME fit (solid line), the FRESCO calculation (dashed line), and the DWBA calculation (dash-dotted line). The error bars represent the statistical and systematic uncertainties.

IV. DISTORTED WAVE BORN APPROXIMATION CALCULATION

Previous low-energy studies at 450 keV [2] have compared the experimental data to the results of a distorted-wave Born approximation (DWBA) calculation which assumes the reaction mechanism is a direct stripping reaction. The elementary picture of a direct (d, n) reaction is one in which the proton is "stripped" from the incoming deuteron, leaving the remaining neutron relatively undisturbed. Direct reactions are generally characterized by surface processes, involving a transition directly from the initial to final state without forming a compound state in the interim [13]. The FORTRAN

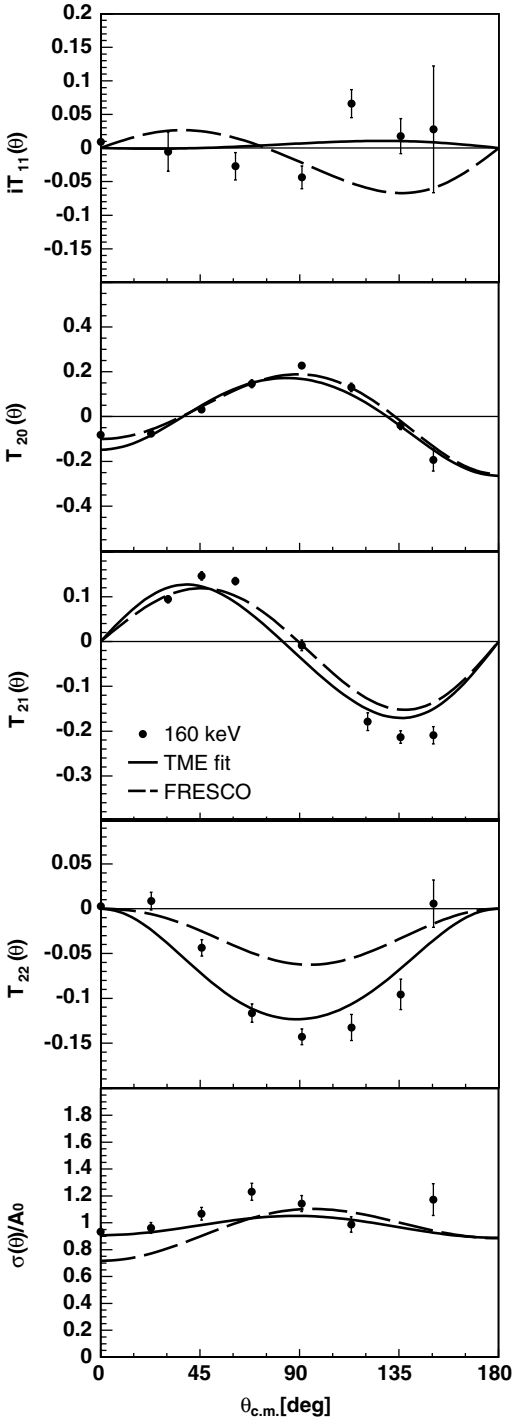

FIG. 4. Experimental data for the ^{7}Li($\vec{d}, n_1$)^{8}Be reaction E_d = 160 keV with the results of a TME fit (solid line) and the FRESCO calculations (dashed line). The error bars represent the statistical and systematic uncertainties.

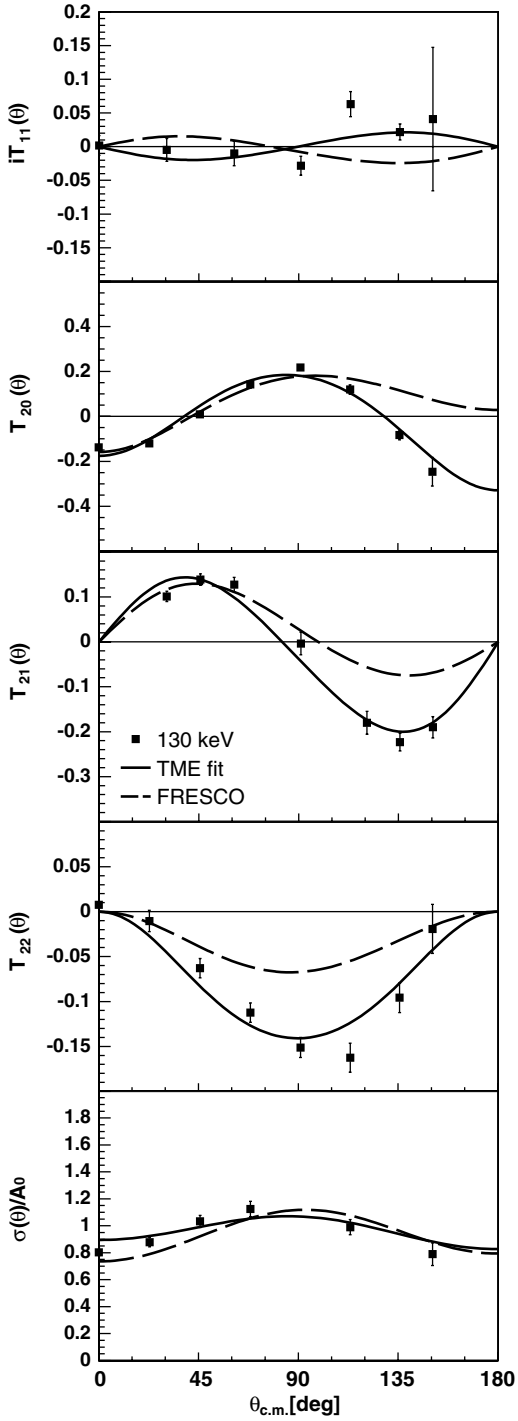

FIG. 5. Experimental data for the ^{7}Li($\vec{d}, n_1$)^{8}Be reaction E_d = 130 keV with the results of a TME fit (solid line) and the FRESCO calculations (dashed line). The error bars represent the statistical and systematic uncertainties.

code DWUCK4 [14] calculates the reaction observables using DWBA and a zero-range interaction. The code is written for projectiles with any combination of spins 0, 1/2, or 1 and computes both the cross section and polarization observables.

The input parameters used to run DWUCK4 for the ^{7}Li(d, n_0)^{8}B reaction at E_d = 160 keV, 130 keV, and 80 keV are given in Table III [15]. The values in column four represent the optical model potential for a deuteron incident on ^{7}Li taken from Ref. [2], and those in column five represent the potential for a neutron on ^{8}Be (the outgoing channel). The values in the sixth column are for the single particle state. The real potential depth value is the starting value which DWUCK4

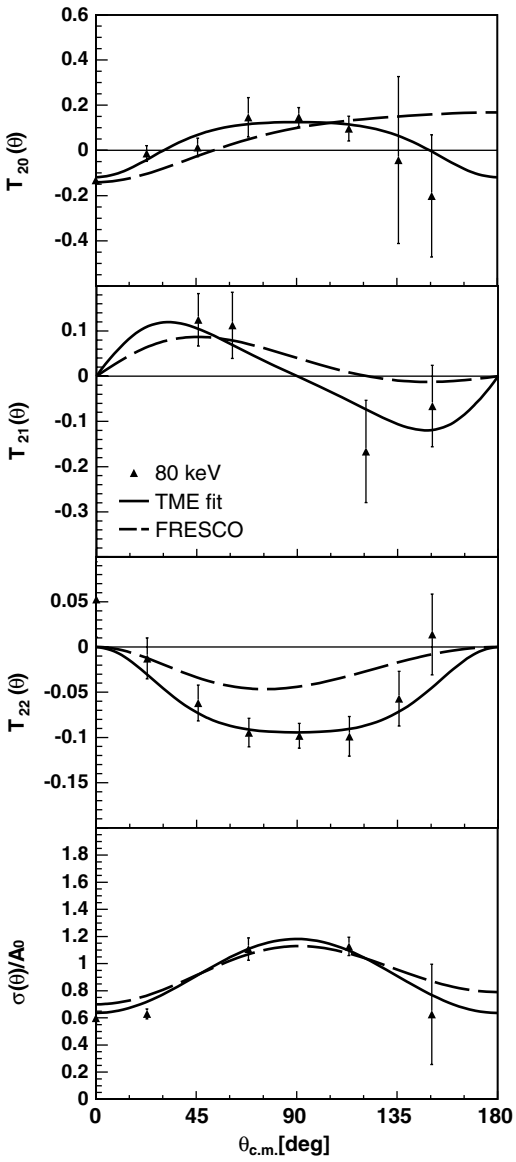

FIG. 6. Experimental data for the ^{7}Li($\vec{d}, n_1$)^{8}Be reaction at $E_d =$ 80 keV with the results of a TME fit (solid line) and the FRESCO calculation (dashed line). The error bars represent the statistical and systematic uncertainties.

then searches on to give the proper binding energy of the single particle state, i.e., the well-depth of the potential is varied to generate the correct ϕ_m^ℓ. The value for the depth in parentheses is the best fit value. In addition, the Coulomb potential is included in all cases with the specified radius. The values used for the binding energy, the orbital angular momentum ℓ, the total angular momentum J, and the number of nodes (excluding the origin and infinity) for the single particle state are also given in Table III. The final well-depth value for the transferred proton is unusually large as a result of the small value of the radius. This value was used because of the success Galloway *et al.*, obtained when fitting cross section data below 500 keV to DWBA calculations using these parameters.

Unfortunately, the results of the calculation did not represent the ^{7}Li(d, n_0)^{8}Be experimental data, especially in the case of the analyzing powers (for example, iT_{11} at $E_d = 130$ and 160 keV), as can be seen in Figs. 1–3. The discrepancy between the data and theory could arise from the theory assuming a pure "direct reaction" mechanism, thus neglecting compound nucleus formation and statistical compound reactions. In addition, in the present DWBA approach, two-step processes, such as those arising from the excitation of the first excited states of the target and residual nuclei have been neglected. This motivated us to look for an alternative theoretical formulation to explain the data, at least one which took two-step processes into account.

V. COUPLED REACTION CHANNELS CALCULATION

As described in detail in Sec. IV, the distorted-waves method is built on the idea that elastic scattering is dominant and must be treated fully while nonelastic events can be treated with perturbation theory. However, a particular nonelastic channel may be sufficiently excited to make perturbation theory inadequate [13].

In a special case of the CRC method, a two-step process becomes important in which a transfer or rearrangement is preceded or followed by an inelastic excitation. This calculation can be carried out to second order in the DWBA and is called the "two-step" DWBA. The elastic distorted waves are replaced by the solutions of the coupled-channels problem to include both elastic and inelastic waves, although the transfer is still treated to first order in the interaction. The reaction may proceed to a given final state along several paths, so the interference between contributions becomes important [13].

The coupled-channels code FRESCO can calculate finite-range transfer interactions among any number of mass partitions and any number of nuclear excitations in each of those partitions [16]. Kernels of the non-local interactions are calculated before the coupled-channels set of equations is solved iteratively. The stored kernels are used at each iteration to integrate the wave functions to generate the source terms for the next iteration [16].

For the ^{7}Li(d, n_0)^{8}Be and ^{7}Li(d, n_1)^{8}Be reactions, the entrance channel was modeled with a potential containing volume, surface imaginary, and spin-orbit terms, as in Galloway *et al.* [2]. However, this did not allow for a correct description of the polarization observables. Inclusion of a target spin-orbit interaction $\mathbf{L} \cdot \mathbf{J}_t$, where L is the orbital angular momentum and J_t is the target spin, in the complete Hamiltonian provided improvement in describing these observables, especially the sign and magnitude of iT_{11}. The same result can be achieved by including a coupling to the first excited state of the target. The effect is due to the existence of low-lying states in the target nucleus with a well-defined $(t + \alpha)$ cluster structure and involves primarily the central parts of the cluster-deuteron potentials [17]. In the present work, these two mechanisms were both included and adjusted to provide the best fit and the most physical parameters. The resulting values for the potentials that best fit the experimental data are given in Table IV, as well as the deformation parameter β. The value

TABLE III. Input parameters for the DWBA code DWUCK4 for the ^{7}Li$(d, n_0)^8$Be reaction. The real potential well-depth value in the "Transferred p" column is the starting value. DWUCK4 searched on the starting value in order to obtain the proper binding energy of the single particle state; the value in parenthesis is the best fit value.

Potential			Incident d	Emitted n	Transferred p
Real					
Depth	V	(MeV)	140.0	46.3	55.0 (81.6)
Radius	r	(fm)	1.80	1.32	1.20
Diffuseness	a	(fm)	1.40	0.66	0.70
Volume imaginary					
Depth	W	(MeV)	30.0	0.75	
Radius	r_w	(fm)	0.84	1.26	
Diffuseness	a_w	(fm)	0.85	0.58	
Surface imaginary					
Depth	W_D	(MeV)	6.87	8.10	
Radius	r_D	(fm)	1.98	1.26	
Diffuseness	a_D	(fm)	0.59	0.48	
Spin-orbit					
Real depth	V_s	(MeV)	4.25	9.00	6.25
Radius	r_s	(fm)	1.00	1.01	1.20
Diffuseness	a_s	(fm)	0.94	0.75	0.70
Coulomb radius	R_c	(fm)	1.30	1.30	1.27
Binding Energy		(MeV)			17.25
Orbital ang. mom.	ℓ				1
Total ang. mom.	J				3/2
Number of nodes					0

of β was allowed to vary to fit the data; the final value of 1.3 given in Table IV is nearly two times larger than the previously determined value of 0.75 [18].

The target spin-orbit potential depth required to fit the data is very large, nearly 8 MeV. Because the interaction strength is proportional to $(\hbar/(2m))^2$, the term would normally be expected to be on the order of 1–2 MeV, given the spin-orbit terms for the other particles. This large spin-orbit strength is unusual but was necessary to reproduce the positive $iT_{11}(\theta)$ values observed in the experiment.

TABLE IV. Values of the potentials used in the CRC code FRESCO for the ^{7}Li$(d, n_0)^8$Be and ^{7}Li$(d, n_1)^8$Be reactions that best reproduced the experimental data.

Potential			Incident d	Emitted n	Transferred p	Target spin-orbit
Real						
Depth	V	(MeV)	149.9	46.3	55.0	
Radius	r	(fm)	2.06	1.32	1.20	
Diffuseness	a	(fm)	0.83	0.66	0.70	
Volume imaginary						
Depth	W	(MeV)	2.30	0.75		
Radius	r_w	(fm)	0.10	1.26		
Diffuseness	a_w	(fm)	0.07	0.58		
Surface imaginary						
Depth	W_D	(MeV)	6.87	8.10	2.70	
Radius	r_D	(fm)	1.98	1.26	0.68	
Diffuseness	a_D	(fm)	0.59	0.48	0.08	
Spin-orbit						
Real depth	V_s	(MeV)	8.50	9.00	3.05	7.91
Radius	r_s	(fm)	1.00	1.01	1.73	0.71
Diffuseness	a_s	(fm)	0.94	0.75	0.70	0.43
Deformation	β	(fm)				1.32

TABLE V. Comparison of the TME fits to the ^{7}Li$(d, n_0)^8$Be data to the results of a coupled reaction channels (CRC) calculation performed using FRESCO.

Transition	$E_d = 160$ keV		$E_d = 130$ keV		$E_d = 80$ keV	
	Strength (%)					
	TME fit	CRC	TME fit	CRC	TME fit	CRC
S-wave	11 ± 2	17	8 ± 1	18	11 ± 1	20
P-wave	75 ± 10	26	86 ± 10	34	84 ± 3	46
D-wave	14 ± 4	57	6 ± 3	48	5 ± 1	34

A two-step DWBA approach, utilizing FRESCO, was used where excitations to the $J^\pi = 1/2^-$ state of ^{7}Li were considered as well as couplings to the $J^\pi = 2^+$ first excited state of ^{8}Be [19]. The results of the calculation compared with the experimental data are shown in Figs. 1–6 for each neutron state and beam energy. It is obvious from these figures that although the FRESCO code is able to qualitatively describe the data, serious discrepancies remain. A comparison of the experimental TMEs with those generated by FRESCO, as described below, confirms this.

The results of the overall s-, p-, and d-wave contributions for each reaction for the calculation and experiment are compared in Tables V and VI and shown in Figs. 7 and 8. For the ^{7}Li$(d, n_0)^8$Be reaction, FRESCO predicts large d-wave contributions which are dominant at $E_d = 160$ keV and 130 keV. However, the experimental results indicate that the reaction proceeds primarily by p-waves in the entrance channel. In the case of the ^{7}Li$(d, n_1)^8$Be reaction, both FRESCO and the experimental results indicate that the reaction mechanism is predominantly p-waves in the entrance channel. FRESCO and the experiment are in good agreement at $E_d = 80$ keV, with the FRESCO result of 93% p-waves lying within the experimental error bars of 99±19%. However, the CRC method predicts that there may be a d-wave contribution, particularly at $E_d =$ 160 keV, which is not observed in the data.

Although the CRC method allows for two-step direct reaction processes, the discrepancies between theory and experiment may arise as a result of the neglect of coupling to other channels in addition to the first excited states. Also, as was the case with the one-step DWBA calculations, CRC assumes a pure "direct reaction" mechanism which neglects possible compound nucleus formation and statistical compound reactions. In addition, the interaction

TABLE VI. Comparison of the TME fits to the ^{7}Li$(d, n_1)^8$Be data to the results of a coupled reaction channels (CRC) calculation done by FRESCO.

Transition	$E_d = 160$ keV		$E_d = 130$ keV		$E_d = 80$ keV	
	Strength (%)					
	TME fit	CRC	TME fit	CRC	TME fit	CRC
S-wave	46 ± 5	9	33 ± 13	2	1 ± 19	3
P-wave	54 ± 7	64	67 ± 11	93	99 ± 19	93
D-wave	–	27	–	5	–	4

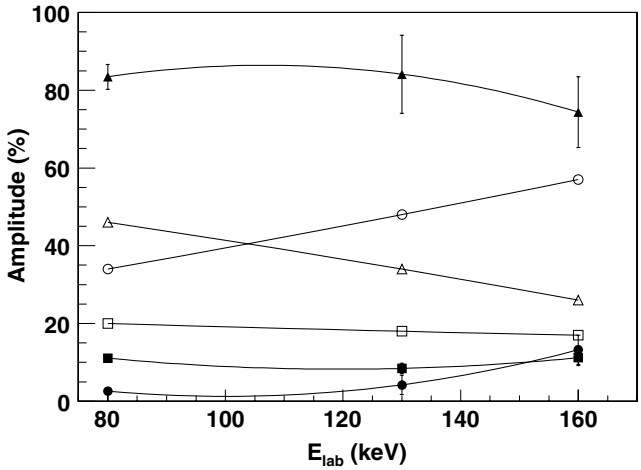

FIG. 7. Total s-, p-, and d-wave contributions for the ^{7}Li$(\vec{d}, n_0)^8$Be reaction as a function of energy. The solid points (■ = s-wave, ▲ = p-wave, ● = d-wave) represent the TME fits to the experimental data, where the error bars represent the errors in the fits. The open points (□ = s-wave, △ = p-wave, ○ = d-wave) represent the results of a CRC calculation. The lines are to guide the eye only.

Hamiltonian used by the theory may not be adequate to describe the reaction. Tensor force effects, such as the D-state component of the deuteron, are not considered. This could be especially important in describing the tensor analyzing powers. In addition, the alpha-triton cluster structure of the ground state of ^{7}Li target is not included in the present model.

VI. CONCLUSION

The polarization observables $iT_{11}(\theta)$, $T_{20}(\theta)$, $T_{21}(\theta)$, $T_{22}(\theta)$, and the differential cross section were measured for both the

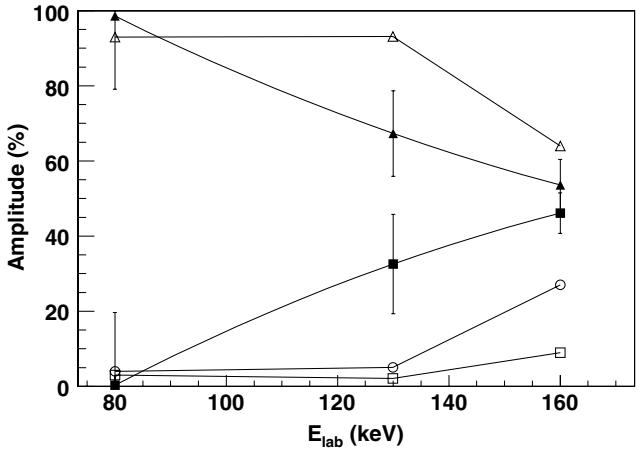

FIG. 8. Total s-, p-, and d-wave contributions for the ^{7}Li$(\vec{d}, n_1)^8$Be reaction as a function of energy. The solid points (■ = s-wave, ▲ = p-wave) represent the TME fits to the experimental data, where the error bars represent the errors in the fits. The open points (□ = s-wave, △ = p-wave, ○ = d-wave) represent the results of a CRC calculation. The lines are to guide the eye only.

TABLE VII. Legendre polynomial fits of order $k = 4$ to the ^{7}Li$(d, n_0)^8$Be data.

Coefficient	160 keV	130 keV	80 keV
A_0	5.676 ± 0.113	7.170 ± 0.063	11.389 ± 0.194
a_1	0.681 ± 0.035	0.670 ± 0.016	1.105 ± 0.033
a_2	0.154 ± 0.042	0.215 ± 0.016	0.272 ± 0.034
a_3	-0.129 ± 0.056	0.024 ± 0.023	0.371 ± 0.052
a_4	0.024 ± 0.064	-0.109 ± 0.029	0.261 ± 0.063
b_1	0.624 ± 0.030	0.505 ± 0.019	
b_2	0.196 ± 0.023	0.123 ± 0.015	
b_3	0.059 ± 0.017	0.045 ± 0.011	
b_4	-0.042 ± 0.016	-0.014 ± 0.012	
c_0	-0.101 ± 0.009	-0.098 ± 0.009	-0.051 ± 0.024
c_1	-0.070 ± 0.018	-0.067 ± 0.020	-0.135 ± 0.038
c_2	-0.171 ± 0.020	-0.202 ± 0.022	-0.074 ± 0.044
c_3	0.136 ± 0.027	0.099 ± 0.030	0.154 ± 0.063
c_4	0.045 ± 0.028	0.132 ± 0.029	0.149 ± 0.056
d_1	0.131 ± 0.016	0.084 ± 0.023	0.162 ± 0.199
d_2	0.186 ± 0.010	0.198 ± 0.013	0.164 ± 0.060
d_3	-0.046 ± 0.008	-0.059 ± 0.011	-0.069 ± 0.119
d_4	-0.042 ± 0.008	-0.054 ± 0.011	-0.100 ± 0.073
e_2	-0.129 ± 0.007	-0.105 ± 0.005	-0.061 ± 0.007
e_3	0.019 ± 0.003	0.022 ± 0.003	0.018 ± 0.004
e_4	0.010 ± 0.002	0.007 ± 0.002	0.014 ± 0.002
χ^2/ν	0.6	2.0	2.8

TABLE VIII. Legendre polynomial fits of order $k = 2$ to the ^{7}Li$(d, n_1)^8$Be data.

Coefficient	160 keV	130 keV	80 keV
A_0	9.117 ± 0.275	8.946 ± 0.232	7.925 ± 0.286
a_1	0.235 ± 0.074	0.104 ± 0.042	-0.065 ± 0.098
a_2	-0.319 ± 0.063	-0.292 ± 0.044	-0.371 ± 0.099
b_1	-0.018 ± 0.021	-0.003 ± 0.016	
b_2	-0.041 ± 0.016	-0.025 ± 0.010	
c_0	0.086 ± 0.008	0.066 ± 0.008	0.073 ± 0.032
c_1	0.056 ± 0.011	0.064 ± 0.013	0.023 ± 0.075
c_2	-0.260 ± 0.017	-0.287 ± 0.017	-0.157 ± 0.067
d_1	-0.006 ± 0.015	-0.057 ± 0.020	0.007 ± 0.114
d_2	0.210 ± 0.011	0.208 ± 0.012	0.150 ± 0.060
e_2	-0.099 ± 0.006	-0.108 ± 0.006	-0.079 ± 0.008
χ^2/ν	3.1	2.4	0.56

^{7}Li$(d, n_0)^8$Be and ^{7}Li$(d, n_1)^8$Be reactions at $E_d = 80$ keV, 130 keV, and 160 keV. A TME analysis yielded a unique, dominant p-wave solution in both the n_0 and n_1 cases. The solution for the n_0 transition corresponded to an average over energy of 82% p-waves in the entrance channel, 10% s-waves, and 8% d-waves, with the $^2p_2$ transition matrix element carrying over 50% of the total strength. The n_1 solution was dominated by an average of 73% p-waves and 27% s-waves, with the $^6p_4$ and $^6p_6$ transition matrix elements carrying over 40% of the total strength.

A DWBA calculation was compared with the experimental data but was unable to reproduce the angular distributions of the analyzing powers. The CRC calculation using the code FRESCO provided a better description of the experimental results than the DWBA calculation once a large target spin-orbit potential and coupling to the first excited state of the target was included in the calculation. However, although the FRESCO result was in qualitative agreement with the experimental data, serious discrepancies remain. A more demanding comparison of the experimentally determined TMEs with the theoretical ones indicated that the theory fails to reproduce significant features of the data. The FRESCO calculations produced a TME result for the n_0 state consisting of an average of 46% d-wave contribution in the entrance channel, 35% p-waves, and 18% s-waves and a result for the n_1 state consisting of an average of 83% p-waves, 12% d-waves, and 5% s-waves. Although the n_1 result is similar to the result obtained from the TME analysis of the data with a dominant p-wave solution (no d-waves were fit to the experimental data), the n_0 result is distinctly different with its dominant d-wave result as opposed to the experimental data's dominant p-wave solution.

ACKNOWLEDGMENTS

The authors would like to thank P. D. Kunz at the Colorado School of Mines for his invaluable help with the DWUCK4 code. One of the authors (N.K.) would like to thank the Triangle Universities Nuclear Laboratory and Duke University for their warm hospitality and support during his stay in the United States. He also would like to acknowledge the financial support of the Dutch Organization for Scientific Research (NWO). This work was partially supported by grants from the U.S. Department of Energy under grant numbers DE-FG02-97ER41046, DE-FG02-97ER41033, and DE-FG02-97ER41042.

APPENDIX: INDIVIDUAL LEGENDRE POLYNOMIAL FITS

The cross section and analyzing powers were expanded in terms of Legendre polynomials according the formalism described in Ref. [7] for both the ^{7}Li$(d, n_0)^8$Be and ^{7}Li$(d, n_1)^8$Be reactions. To obtain the best fit, it was necessary to expand the ^{7}Li$(d, n_0)^8$Be reaction to order $k = 4$ and the ^{7}Li$(d, n_1)^8$Be reaction to order $k = 2$. The values of the coefficients from those expansions are given in Tables VII and VIII. In both cases, there are no b coefficients for $E_d = 80$ keV because there was no $iT_{11}(\theta)$ data at that energy.

[1] R. N. Boyd, C. A. Mitchell, and B. S. Meyer, Phys. Rev. C **47**, 2369 (1993).
[2] R. B. Galloway and A. M. Ghazarian, Phys. Rev. C **29**, 2349 (1984).
[3] U. von Möllendorff, A. Janett, F. Seiler, and H. R. Striebel, Nucl. Phys. **A209**, 323 (1973).
[4] A. Sabourov, M. W. Ahmed, M. A. Blackston, A. S. Crowell, C. R. Howell, B. A. Purdue, K. Sabourov, A. Tonchev,

H. R. Weller, R. M. Prior *et al*., Phys. Rev. C **73**, 015801 (2006).
[5] *Polarization Phenomena in Nuclear Reactions*, edited by H. H. Barschall (University of Wisconson Press, Madison, Wisconsin, 1971), p. xxv.
[6] E. A. Wulf, Ph.D. thesis, Duke University (1999).
[7] R. G. Seyler and H. R. Weller, Phys. Rev. C **20**, 453 (1979).
[8] P. R. Bevington and D. K. Robinson, *Data Reduction and Error Analysis for the Physical Sciences* (McGraw-Hill, Inc., New York, 2003).
[9] H. Feschbach, in *Nuclear Spectroscopy*, Part B, edited by F. Ajzenberg-Selove (Academic Press, New York, 1960), p. 625.
[10] T. A. Welton, in *Fast Neutron Physics, Vol. II*, edited by J. B. Marion and J. L. Fowler (Interscience, New York, 1963), p. 1317.
[11] S. Devons and L. J. B. Goldfarb, Handbuch der Physik **42**, 362 (1957).
[12] F. Seiler, Comput. Phys. Commun. **6**, 229 (1974).
[13] G. R. Satchler, *Direct Nuclear Reactions* (Oxford University Press, Oxford, 1983).
[14] P. D. Kunz, http://spot.colorado.edu/∼kunz/DWBA.html.
[15] P. D. Kunz (private communications 2003).
[16] I. J. Thompson, http://www.fresco.org.uk (2004).
[17] H. Nishioka, R. C. Johnson, J. A. Tostevin, and K. I. Kubo, Phys. Rev. Lett. **48**, 1795 (1982).
[18] T. Belgya, O. Bersillon, R. Capote, T. Fukahori, G. Zhigang, S. Goriely, M. Herman, A. V. Ignatyuk, S. Kailas, A. Konig, *et al*., *Handbook for calculations of nuclear reaction data: Reference Input Parameter Library* (IAEA, Vienna, 2005), http://www-nds.iaea.org/RIPL-2/.
[19] B. Braizinha, H. R. Weller, A. Sabourov, and I. J. Thompson, Triangle Universities Nuclear Laboratory Progress Report XLIV (2005).